INFLUENCE OF HEAT INPUT ON THE TENSILE PROPERTIES OF AUSTENITIC-FERRITIC WELDED JOINTS

Aleksandar G. Bukvić[a], *Dalibor* P. Petrović[b],
Igor Z. Radisavljević[c], *Saša* S. Dimitrić[d]

[a] University of Defense in Belgrade, Military Academy,
   Belgrade, Republic of Serbia,
   e-mail: a_bukvic@yahoo.com, **corresponding author**,
   ORCID iD: https://orcid.org/0000-0002-3025-8446

[b] University of Defense in Belgrade, Military Academy,
   Belgrade, Republic of Serbia,
   e-mail: dalibor.petrovic140@gmail.com,
   ORCID iD: https://orcid.org/0000-0001-6092-5695

[c] Ministry of Defense of the Republic of Serbia,
   Military Technical Institute, Belgrade, Republic of Serbia,
   e-mail: radisavljevicigorbg@gmail.com,
   ORCID iD: https://orcid.org/0000-0002-8523-0993

[d] University of Defense in Belgrade, Military Academy,
   Belgrade, Republic of Serbia,
   e-mail: sasa.dimitric@mod.gov.rs,
   ORCID iD: https://orcid.org/0000-0003-3547-7047

Abstract:

Introduction/purpose: During exploitation tests of gasoline storage tanks, cracks can form in an austenitic-ferrite welded joint, which can compromise the entire tank.

Methods: In order to obtain a welded joint of satisfactory strength and durability, the paper analyzes the influence of heat input on the tensile characteristics of welded joints. In the current literature and practice, additional materials for welding the tank elements are selected according to the chemical compositions of the elements of basic materials, with the help of the Schaeffler diagram. In this paper, the characteristics of welded joints of gasoline storage tanks are examined, when the largest part of the tank is made of fine - grained microalloyed steel NIOMOL 490 K, while the roof part of the tank is made of austenitic steel. Slabs of these two materials were welded by the MIG process with additional material MIG 18/8/6, at different amounts of heat input.

Conclusion: The analysis of the results obtained by tensile testing according to SRPS EN ISO 6892-1: 2020 standard concluded that the behavior of the joint as a whole depends on the properties of each individual part of the welded joint and their mutual influence. It was also concluded that the mutual influence is better if welding is performed with a lower amount of heat input, because then a lower degree of mixing of additional material with basic materials is achieved.

Key words: austenitic-ferritic welded joint, strength, plasticity.

Introduction

Lack of storage space and obsolescence of the existing tanks for storage of petroleum products call for a rapid construction of new tanks. When designing new tanks, in addition to choosing adequate construction materials, it is necessary to perform adequate welding of the structure, so that during operation there would be no cracks that could lead to accidents with large financial losses and harmful effects on the environment (Jovičić et al, 2006).

In this paper, the characteristics of welded joints are analyzed on the example of tanks whose mantle and battom are made of microalloyed steel S500NL1, under the commercial name NIOMOL 490K, 16 mm thick. The roof covering is made of high-alloy austenitic steel X7CrNiNb18.10 according to EN 10088 (Č.4574 according to JUS C.B0.600) standard, 12 mm thick (Bukvić, 2012).

During exploitation maintenance, cracks were discovered in the welded joint of the casing and the roof covering. The X-ray reveals the cracks shown in Figure 1. Two cracks parallel to the fusion line and two cracks extending radially to the fusion line can be seen in the figure. Cracks parallel to the fusion line are found in the base materials. In welded joints of microalloyed steels, cracks usually occur in the heat affected zone (HAZ) due to structural changes caused by welding. In this case, cracks appeared in the base material, far from the zone in which structural changes occurred during welding. Crack positions indicate that in the combination of the three materials that make up the welded joint, the high-alloy austenitic steel material X7CrNiNb18.10 is weakest when the highest heat input values are entered, and that in the case of the lowest heat input, the base metal S500NL1 is the weakest link.
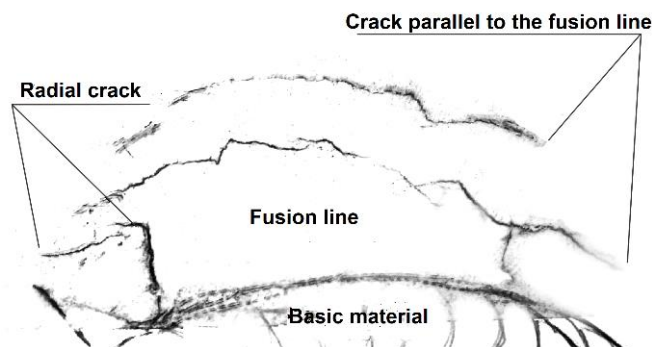
Figure 1 – X-ray of the cracked joint
Рис. 1 – Рентгеновский снимок треснувшего соединения
Слика 1 – Рендгенски снимак споја са прслинама

The metal weld structure of heterogeneous compounds can be roughly predicted using the Schaeffler diagram (Bukvić, 2012). Based on the calculated values of the Cr and Ni equivalents, the position points of the base materials and weld metals are plotted in the Schaeffler diagram shown in Figure 2.
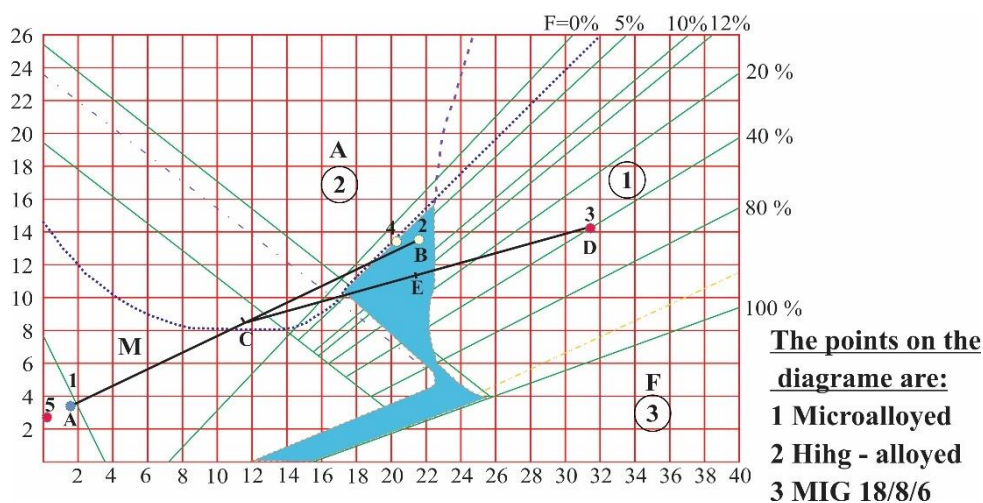
Figure 2 – Positions of the points of the basic and additional materials in the Schaeffler diagram
Рис. 2 – Положения точек основного и дополнительного материалов на диаграмме Шеффлера
Слика 2 – Положаји тачака основних и додатних материјала у Шефлеровом дијаграму

The chemical composition of the weld metal and its structure are chosen on the basis of the Schaeffler diagram so that they are in an area where there is no tendency to defects (hot cracks, martensite formation, brittleness due to grain growth and σ-phase separation). However, the chemical composition of the weld metal is not unique, but represents a series of chemical compositions created by melting the basic materials and the additional material. This is especially pronounced with multi-pass seams.

Welding technology

In order to determine the adequate welding technology which would avoid the appearance of cracks in the welded joint, samples of two welded plates were used. These two experimental plates, marked with numbers 1 and 2, were obtained by welding the basic materials from which the tank was made (microalloyed and high alloy steel). Table 1 shows the chemical compositions of the basic materials.

Table 1 – Chemical composition of the basic materials
Таблица 1 – Химический состав основных материалов
Табела 1 – Хемијски састав основних материјала

Steel	C	Si	Mn	P	S	Cr	Ni	Cu	Al	Mo	Ti	V	Nb
microalloyed	0.10	0.38	0.66	0.014	0.02	0.76	0.10	-	-	0.33	-	0.02	-
high alloy	0,04	0.35	1.73	0.031	0.004	17.9	11.6	0.18	0.061	2.16	0.38	0.079	0.016

Both plates are welded by the MIG process with additional material MIG 18/8/6, but with different amounts of heat input. The selected welding process and the additional material are identical to the connection to which the roof cover and the tank casing are connected. The chemical composition and the mechanical properties of the additional material are given in Tables 2 and 3.

Table 2 – Chemical compositions of the additional material MIG 18/8/6
Таблица 2 – Химические составы дополнительного материала MIG 18/8/6
Табела 2 – Хемијски састави додатног материјала МИГ 18/8/6

	C	Si	Mn	Cr	Ni
MIG 18/8/6	0.08	<1.0	7	18.5	9

Table 3 – Mechanical properties of the pure metal weld from the selected additional material
Таблица 3 – Механические свойства чистого металла сварного шва из выбранного дополнительного материала
Табела 3 – Механичке особине чистог метал шава од одабраног додатног материјала

	R_e, [N/mm²]	R_m, [N/mm²]	A_5, [%]	KV,[J]	
MIG 18/8/6	> 380	560 do 660	35	> 40 (at 20 ⁰C)	

The additional material MIG 18/8/6 is recommended in (Jesenice Ironworks, 2005) in which a high-alloy additional material was used for welding various steels. This choice of additional material is also indicated by the data from the Schaeffler diagram, Figure 2. When choosing the additional material, it was taken into account that it has different values of yield stress and tensile strength in relation to the basic materials. A mixture of Ar gases and 2% O2 was used as a protective atmosphere during welding with the chemical composition given in Table 4.

Table 4 – Chemical composition of the gas mixtures
Таблица 4 – Химический состав газовых смесей
Табела 4 – Хемијски састав мешавина гаса

Content of components in the mixture [vol%]	
O₂	Ar
2.00	Rest

Welding is performed by the electric arc semi-automatic MIG / MAG process, bearing in mind that in recent years the use of the semi-automatic MIG / MAG welding process is increasingly common compared to other welding processes in steel structures.
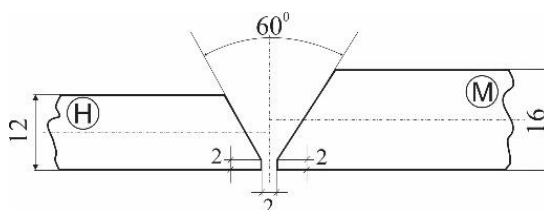
Figure 3 – Shape and dimensions of the "Y" groove
Рис. 3 – Форма и размеры канавки "Y"
Слика 3 – Облик и димензије „Y" жлеба

The MIG / MAG welding device KEMPACT 3000+ FastMig 400 was used for welding. The preheating temperature of 60 ^{0}C and the intermediate temperature of 60 ± 10 ^{0}C were adopted (Bukvić, 2012).
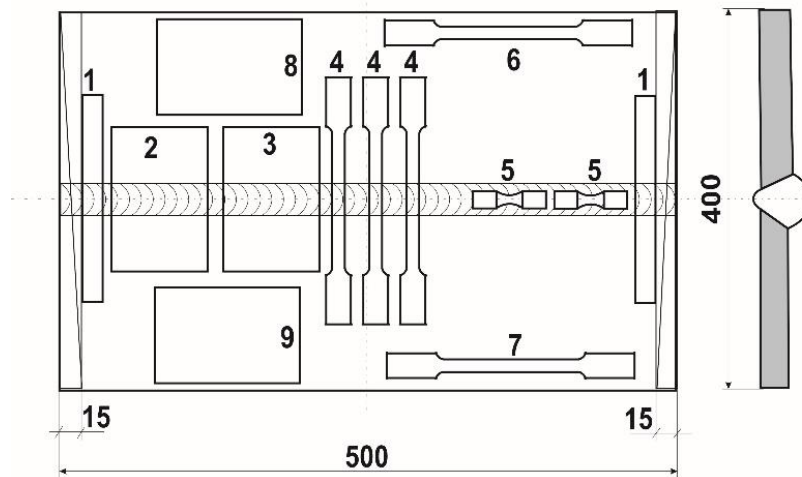
Figure 4 – Appearance of the welded plate scheme and the test tube cutting plan
Рис. 4 – Вид схемы сварной пластины и план резки эпруветки
Слика 4 – Изглед шеме заварених плоча и план исецања епрувета

The obtained welded experimental plates 1 and 2 have dimensions of 500 x 400 mm with the "Y" groove, as shown in Figure 3. Test tubes were cut from the obtained plates and the scheme of cutting tubes from the welded plates for testing the characteristics of strength, plasticity, as well as for microstructural tests and hardness tests, is shown in Figure 4.

The plates were preheated and the intermediate temperatures were maintained by heating with oxygen and acetylene. Preheating temperatures and intermediate temperatures were controlled by a contact thermometer. Figure 5 shows the layout of laying the additional material during the welding of experimental plates 1 and 2.
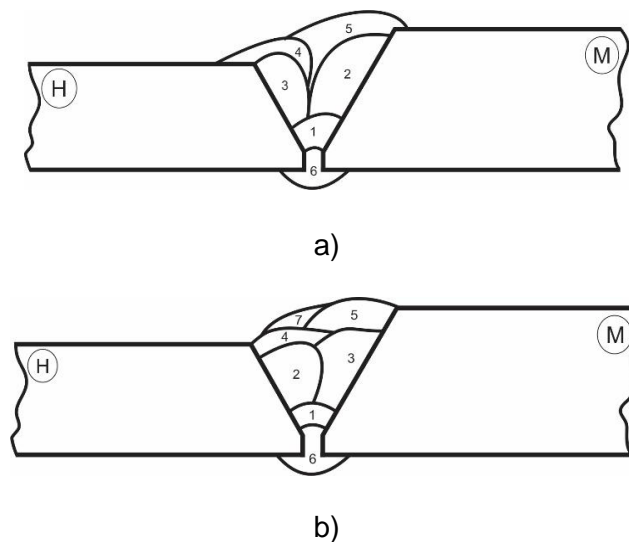
Figure 5 – Welded joint layout diagram for plates 1 and 2:
a) scheme of laying the additional material for plate 1
b) scheme of laying the additional material for plate 2
Рис. 5 – Схема расположения соединений свариваемых пластин 1 и 2:
а) схема сварного соединения пластины 1
б) схема сварного соединения пластины 2
Слика 5 – Шема завареног споја за плоче 1 и 2:
а) шема завареног споја за плочу 1,
б) шема завареног споја за плочу 2

Plate 1 was welded at an average value of the amount of heat input of 8.88 [kJ / cm], as indicated in the last column of Table 5. The upper (maximum) limit value of the amount of heat input for the selected welding process was used for welding this plate and the additional material.

Plate 2 was welded at an average heat input of 6.87 [kJ / cm] (see last column of Table 6). In plate 2, welding was performed with the lower (minimum) limit value of the amount of heat input for the selected welding procedure and the additional material.

Welding procedures are described in the literature (Bukvić, 2012) for both welded plates.

After welding, plates 1 and 2 were inspected and subjected to non-destructive testing. Radiographic irradiation with γ-rays did not reveal any defects in the joints, such as: cracks, porosity, non-penetration, sticking, edge joints and the like.

Table 5 – Passages when welding plate 1 with the amounts of heat input
Таблица 5 – Проходы при сварке пластины 1 с учетом количества подведенного тепла
Табела 5 – Пролази при заваривању плоче 1 са количинама унете топлоте

Marking of welding plates and wires	Serial number of welding	Welding		Strength electricity [A]	Voltage [V]	Amount of heat input [kJ/cm]		
		Time [min.]	Speed [cm/min]			Calculated	Real [η=0,6]	Average
Plate 1. wire 18/8/6	1 root	3.30	15.2	132	18.9	9.85	5.91	*8.88*
	2 to M	2.12	23.6	228	27.6	16.00	9.60	
	3 to H	2.33	21.5	237	28.0	18.52	11.11	
	4 to M	2.12	23.6	240	28.3	17.27	10.36	
	5 to H	2.13	23.5	235	28.3	18.06	10.84	
	6 root*	1.33	37.6	210	27.1	9.08	5.45	

* root canal ground and re-welded (marked with 6 root)

Table 6 – Passages when welding plate 2 with the amounts of heat input
Таблица 6 – Проходы при сварке пластины 2 с учетом количества подведенного тепла
Табела 6 – Пролази при заваривању плоче 2 са количинама унете топлоте

Marking of welding plates and wires	Serial number of welding	Welding		Strength electricity [A]	Voltage [V]	Amount of heat input [kJ/cm]		
		Time [min.]	Speed [cm/min]			Calculate	Real [η=0,6]	Average
Plate 2. wire 18/8/6	1 roof	3.55	14.1	135	18.8	10.80	6.48	6.87
	2 ka M	1.73	28.9	218	27.2	12.31	7.39	
	3 ka H	1.75	28.6	230	27.6	13.32	7.99	
	4 ka H	1.37	36.5	230	27.6	10.44	6.26	
	5 ka M	1.88	26.6	220	27.3	13.55	8.13	
	6 root*	1.42	35.2	210	27.1	9.70	5.82	
	7 central	1.43	35.0	215	27.2	10.03	6.02	

* root canal ground and re-welded (marked with 6 root)

Test results

The tensile strength test of the welded joint was performed according to SRPS EN ISO 6892-1: 2020 on smooth flat tubes with parallel sides. The test was performed on a SCHENCK – TREBEL RM 100 ripper. As the plates of both base materials were of different thicknesses (12 and 16 mm), the tubes were machined and reduced to the same thickness to a thinner plate (12mm) to obtain consistent results before the test.

For comparison, the tensile test tubes were cut from the plates of basic materials. Based on the obtained results ($F_{0,2}$, F_m), the resistance properties were calculated: the yield stress $R_{0,2}$ and the tensile strength R_m. The deformation properties were also determined: the elongation A and the contraction Z. Table 7 lists the mechanical properties of microalloyed and high alloy steel.

Table 7 – Mechanical properties of microalloyed and high alloy steel
Таблица 7 – Механические свойства микролегированной и высоколегированной стали
Табела 7 – Механичка својства микролегираног и високолегираног челика

Test tube	Yield stress $R_{0,2}$ [MPa]	Tensile strength R_m[MPa]	Elongation A [%]	Contraction Z [%]
Microalloyed	497	582	21	63
High-alloy	308	573	37	53

Figure 6 shows the σ – ε diagrams for a) microalloyed and b) high-alloy steel.

For microalloyed steel, the σ – ε diagram with a pronounced yield strength was obtained, and for high-alloy steel, the obtained diagram was without a pronounced yield strength.

Two test tubes (Figure 4, test tube number 5) were cut from both plates in the part of the metal seam for tensile characteristics tests. The results of testing the tensile properties of the metal seams for both plates are shown in Table 8.

a)

b)
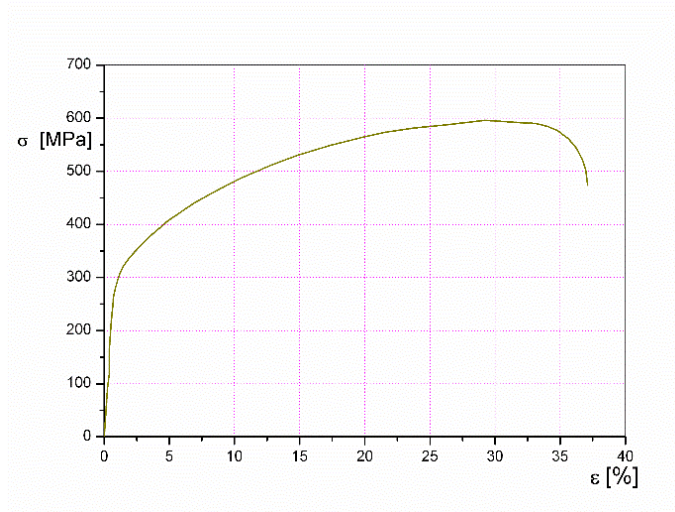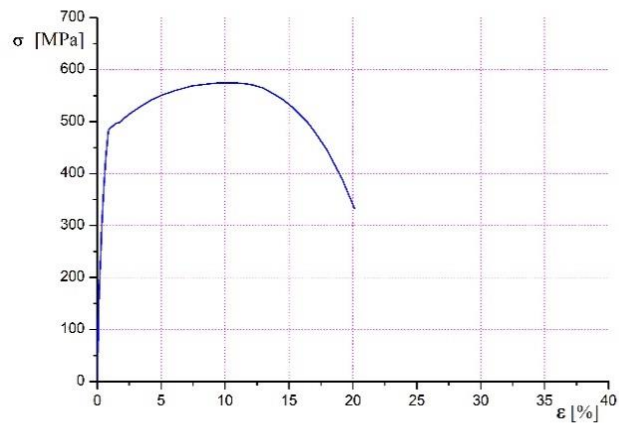
Figure 6 – σ – ε diagrams for the base materials:
a) Microalloyed steel NIOMOL 490K, b) High-alloy steel X7CrNiNb18.10

Рис. 6 – Диаграммы σ – ε основных материалов:
а) Микролегированная сталь NIOMOL 490K,
б) Высоколегированная сталь X7CrNiNb18.10

Слика 6 – Дијаграми σ–ε за основне материјале:
а) микролегирани челик NIOMOL 490K,
б) високолегирани челик X7CrNiNb18.10.

Table 8 – Tensile characteristics of the metal welded tubes on the welded plates
Таблица 8 – Характеристики растяжения эпроветки металлических сварных
швов на сварных пластинах
Табела 8 – Затезне карактеристике епрувета из метал шава по завареним
плочама

Plate	Label on the test tube	Yield stress $R_{p0,2}$ [MPa]		Tensile strength R_m [MPa]		Elongation A [%]	
		$R_{p0,2}$	average value	R_m	average value	A	average value
1	A-2.1	473	466	678	682	43	42
	A-2.4	458		685		41	
2	A-2.2	450	443	678	693	39	39
	A-2.3	436		707		38	

As it can be seen in Table 8, the obtained yield stresses Rp0.2 and the tensile strengths Rm of the metal weld for plates 1 and 2 are similar. This is expected according to (Bukvić, 2012; Kassner, 2015), having in mind that the same basic materials and the same additional material MIG 18/8/6 were used.

After that, three tubes with the marks: 1.1, 1.2 and 1.3 were cut from plate 1, from the part of the plate where the welded joint is located (Figure 4, tubes under number 4). The test results of the joint specimens for plate 1 are given in Table 9, while the σ – ε diagram is shown in Figure 7.
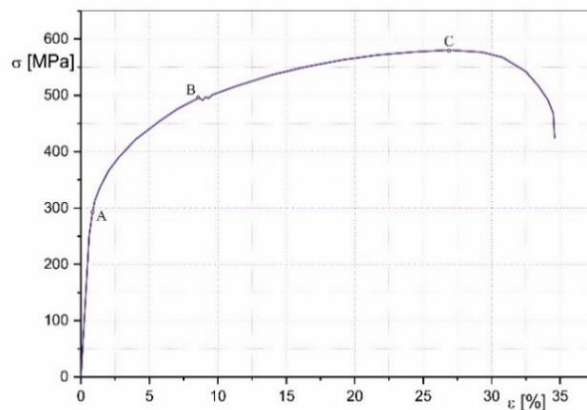
Figure 7 – Diagram σ – ε for test tube 1.1
Рис. 7 – Диаграмма σ – ε эпроветки 1.1
Слика 7 – Дијаграм σ–ε за епрувету 1.1
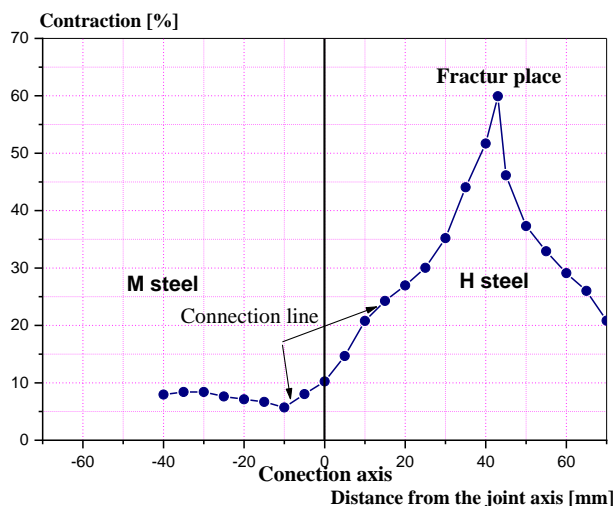
Figure 8 – Change in the contractions of the tube cross section 1.1
Рис. 8 – Изменение сужений поперечного сечения эпроветки 1.1
Слика 8 – Промена контракција попречног пресека епрувете 1.1

Figure 8 shows the change in the contraction of the cross section of test tube 1.1 along its measuring part, and Figure 9 shows the appearance of test tube 1.1 after tearing. The fracture of the test tube is accompanied by uneven deformation of the measured length.
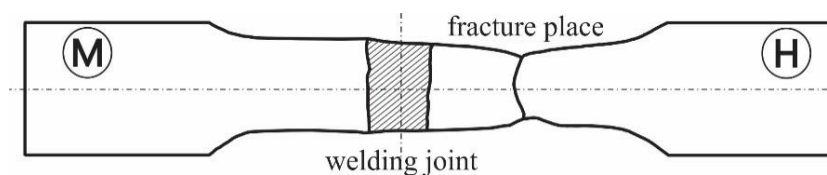
Figure 9 – Test tube 1.1 after tearing
Рис. 9 – Эпроветка 1.1 после разрыва
Слика 9 – Епрувета 1.1 након кидања

The tensile characteristics results for plate 1 for all three tested specimens are shown in Table 9. The points A, B and C are the characteristic points of the σ – ε diagram for specimen 1.1 (see Figure 7).

Table 9 – Tensile characteristics of plate joint tubes 1
Таблица 9 – Характеристики растяжения эпроветки соединения пластины 1
Табела 9 – Затезне карактеристике епрувета споја из плоче 1

Test tube number	Yield stress at the point A [MPa]		Stress at the point B [MPa]		Tensile strength at the point C [MPa]		ε [%]	
	R_A	average value	R_B	average value	R_C	average value		average value
1.1	295		495		580		35	
1.2	311	308	495	497	566	573	35	34
1.3	318		500		574		32	

The mean stress at the point A is 308 MPa, at the point B it is 497 MPa, and at the point C it is 573 MPa, as shown in Table 9. The mean percentage elongation of the tubes is 34%. The fracture occurred in high-alloy steel in all three tubes.

Table 10 compares the stresses at the characteristic points A, B and C of the σ – ε diagram for tube 1.1, according to Figure 7 and Table 9, and the mean stress values for the base materials and the value deviations.

Table 10 – Stress at the characteristic points of the σ – ε diagram for test tube 1.1
Таблица 10 – Напряжение в характерных точках диаграммы σ – ε эпроветки 1.1
Табела 10 – Напон у карактеристичним тачкама дијаграма σ–ε за епрувету 1.1

Stress at the characteristic points A. B i C		Characteristic stress values for basic materials		Deviation Δ R [MPa]	Deviation [%]
Mark	Average stress value. table 9	Mark. table 8	average value stress		
R_A	308	$R_{p0.2}$ steel H	324	16	4.9
R_B	497	$R_{p0.2}$ steel M	491	8	1.6
R_C	573	R_m steel H	595	22	3.4

Observing the changes in cross-sectional contractions along the measuring part of the test tube (Figure 8), it can be seen that the weld metal has a higher cross-sectional contraction than microalloyed steel and the HAZ towards microalloyed steel. The smallest contraction (about 6%) occurs at the fusion line of the metal weld and the microalloyed steel. Fracture occurs in high-alloy steel approximately half the measuring length of the plate 1 tube. The narrowing towards the melting line from the middle of the measuring tube is greater on the high-alloy steel side than the narrowing towards the melting line with the microalloyed steel. The

measurement showed a greater narrowing of the measuring part of the test tube on the high-alloy steel side than the measuring part of the test tube on the micro-alloy steel side.

Three tubes with the marks: 2.1, 2.2 and 2.3 were cut from plate 2, from the part of the plate in which the welded joint is located (Figure 4, tubes under number 4). The test results of the joint test tubes for plate 2 are given in Table 11, while the σ – ε diagram is shown in Figure 10.
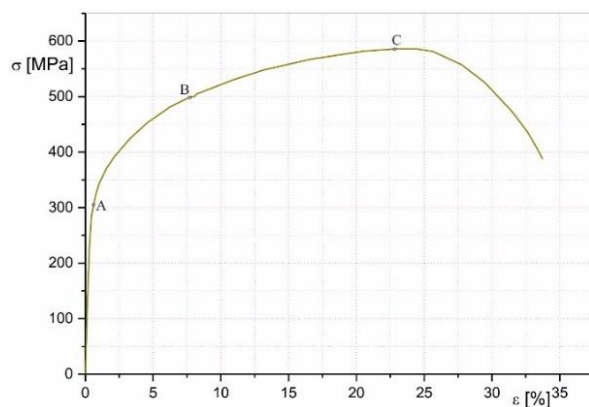
Figure 10 – Diagram σ – ε for test tube 2.1
Рис. 10 – Диаграмма σ – ε эпроветки 2.1
Слика 10 – Дијаграм σ–ε за епрувету 2.1
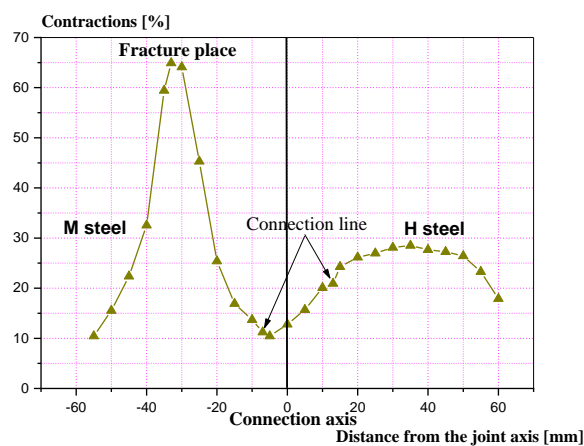
Figure 11 – Change of the contractions of the tube cross-section 2.1
Рис. 11 – Изменение сужений поперечного сечения эпроветки 2.1
Слика 11 – Промена контракција попречног пресека епрувете 2.1

Figure 11 shows the change in the contractions of the cross section of tube 2.1 along its measuring part, and Figure 12 shows the appearance of tube 2.1 after tearing. The fracture of the test tube is accompanied by uneven deformation of the measured length.
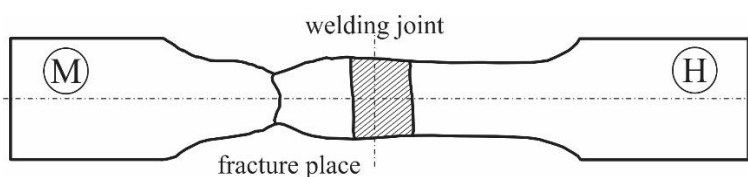
Figure 12 – Test tube 2.1 after tearing
Рис. 12 – Эпроветка 2.1 после разрыва
Слика 12 – Епрувета 2.1 након кидања

The results of the tensile characteristics of the joint for plate 2 for all three tested specimens are given in Table 11.

Table 11 – Tensile characteristics of plate joint tubes 2
Таблица 11 – Характеристики растяжения эпроветки соединения пластины 2
Табела 11 – Затезне карактеристике епрувета споја из плоче 2

Test tube number	Yield stress at the point A [MPa]		Stress at the point B [MPa]		Tensile strength at the point C [MPa]		E [%]	
	R_A	average value	R_B	average value	R_C	average value		average value
2.1	318		512		588		37	
2.2	315	309	499	501	586	586	34	36
2.3	295		493		583		36	

The average stress value at the point A is 309 MPa, at the point B is 501 MPa, and at the point C is 586 MPa, as shown in Table 11. The average value of the percentage elongation of the tubes is 36 %. Fracture occurred in microalloyed steel in all three tubes.

Table 12 compares the stresses at the characteristic points of the σ – ε diagram for tube 2.1, according to Figure 10 and Table 9, and the mean stress values for the base materials and the value deviations.

Table 12 – Stresses at the characteristic points of the σ – ε diagram for test tube 2.1
Таблица 12 – Напряжения в характерных точках диаграммы σ – ε эпроветки 2.1
Табела 12 – Напони у карактеристичним тачкама дијаграма σ–ε за епрувету 2.1

Stress at the characteristic points in Figure 10		Characteristic stress values for basic materials		Deviation Δ R [MPa]	Deviation [%]
Mark	Average stress value. Table 9	Mark. Table 8	Average stress value		
R_A	309	$R_{p0.2}$ steel H	324	15	4.6
R_B	501	$R_{p0.2}$ steel M	491	10	2.0
R_C	586	R_m steel M	583	3	0.5

The examination of the test tubes and the analysis of Figure 11 show that the smallest cross-sectional contraction (about 10%) occurs at the fusion line of the metal weld and the microalloyed steel. The fracture occurred in the microalloyed steel, approximately half of the measuring length of the tube on the side of the microalloyed steel. The narrowing towards the fusion lines with base materials is greater on the high-alloy steel side than on the fusion line with the micro-alloy steel. The total narrowing of the cross section of the measuring lengths of the base materials is greater on the side of the microalloyed steel.

Both experimental plates 1 and 2 were subjected to hardness tests of all characteristic structures located on them. The results of the hardness measurements and the microstructure tests show the usual values for the steels used (Bukvić, 2012).

a)   b)
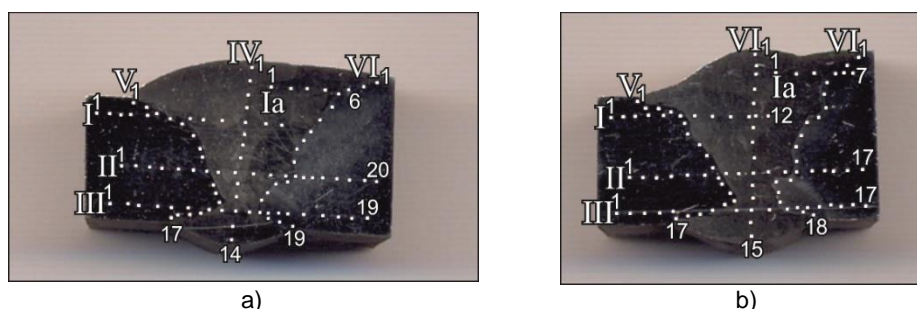
Figure 13 – Macroscopic image of the welded plates with impressions from the hardness measurements:
a) Macroscopic image of plate 1, b) Macroscopic image of plate 2
Рис. 13 – Макроскопический снимок сварных пластин с отпечатками измерений твердости:
a) Макроскопический снимок пластины 1, б) Макроскопический снимок пластины 2
Слика 13 – Макроскопски снимак заварених плоча са отисцима од мерења тврдоће:
a) макроскопски снимак плоче 1, б) макроскопски снимак плоче 2
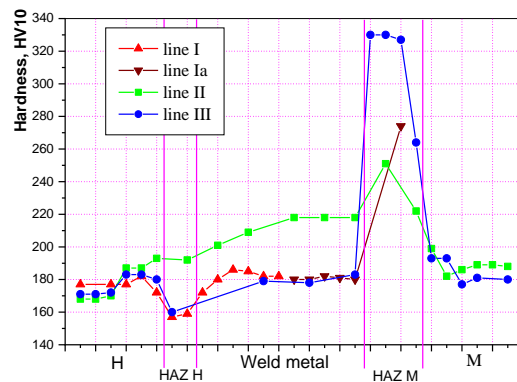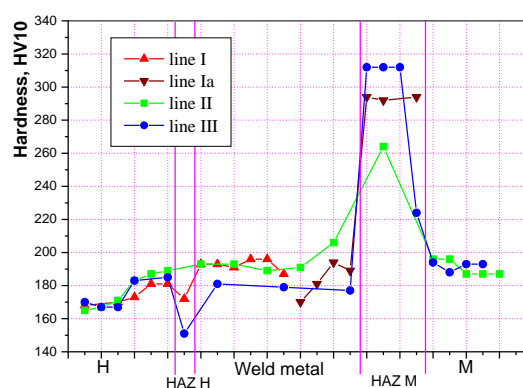
Figure 14 – Graphic representations of the material hardness change in plates 1 and 2 by zones:
a) Change in hardness in plate 1
b) Change in hardness in plate 2
Рис. 14 – Графические изображения изменения твердости материала пластин 1 и 2 по зонам:
а) Изменение твердости пластины 1
б) Изменение твердости пластины 2
Слика 14 – Графички прикази промене тврдоће материјала у плочама 1 и 2 по зонама:
а) промена тврдоће у плочи 1,
б) промена тврдоће у плочи 2

According to the macroscopic image of plate 1 (Figure 13 under a), the hardness of the HAZ towards high-alloy steel (153–192 HV) does not differ significantly from the hardness of high-alloy steel (168–193 HV). As it can be seen from Figure 14 under a, the HAZ hardness values for microalloyed steel (199–333 HV) are higher than the hardness values of microalloyed steel (180–193 HV). The metal weld structure is austenitic with about 30% δ ferrite (Guo et al, 2015; Liu & Pons, 2017).

The test results of the joint from plate 2 according to the shown macroscopic image (Figure 13 under b), show that, similarly to plate 1, the values of the HAZ hardness towards high-alloy steel (151–192 HV) do not differ significantly from the hardness values of high-alloy steel (165– 189 HV). The values of the HAZ hardness towards microalloyed steel (224–333 HV) are higher than the hardness values of microalloyed steel (187–196 HV) and beinite was observed, Figure 14 under b (Guo et al, 2015; Liu & Pons, 2018).

Analysis of results

Plates 1 and 2 are welded with the maximum and minimum allowable amount of heat input. The values of the amount of heat input used in this case represent the limit values for the selected welding process and additional material. Tables 6 and 7 show that the input difference is about 30%. A lower amount of heat input would be achieved by reducing the current or by increasing the welding speed. Decreasing the current leads to the appearance of an unstable arc, and increasing the welding speed leads to poorer formation of metal seams. In both cases, unacceptable errors in the formation of metal seams (eg porosity, gluing) occur (Miletić et al, 2020; Zhang et al, 2015; Durmusoglu et al, 2015). Higher heat input would be achieved by increasing the current or reducing the welding speed. Increasing the welding current leads to the overheating of the liquid metal and poorer weld formation, and reducing the welding speed leads to a large volume of liquid metal that is difficult to control.

According to Schaeffler's diagram (Figure 2), in the welding of the used base materials (microalloyed ferritic-perlite and high-alloy austenitic steel) it is possible to use additional material MIG 18/8/6, because the result of this joint is in the safe area (Miletić et al, 2020; Zhang et al, 2015; Durmusoglu et al, 2015).

After welding, visual and radiographic control of all welded plates was performed. No errors were observed on either plate 1 or plate 2.

The results of hardness measurements on both experimental plates were obtained by the Vickers method at 10 daN. It is noticed that in plates

1 and 2 the highest values of hardness are achieved in the HAZ from microalloyed steel. In this coarse-grained zone, there was a large increase in grain, whereby the ferritic-perlite structure of microalloyed steel changed to beinitic. Microalloyed steel has higher hardness values on both welded plates than austenitic high alloy steel and its HAZ. The metal hardness values are higher than those of both base materials in all cases. The lowest values of hardness were shown by the HAZ on the part of high-alloy steel, except for plate 1, where the values are approximately the same as the values of high-alloy steel. The decrease in hardness in the HAZ of high-alloy steel was due to the increase in grain in the HAZ (Miletić et al, 2020; Sankar et al, 2021).

The obtained tensile diagrams of the metal weld tubes for plates 1 and 2 are typical for austenitic steels. When compared, the values of the tensile strength and the yield stress for additional material MIG 18/8/6 differ somewhat from the values offered by the manufacturer. The obtained values of the tensile strength Rm for additional material 18/8/6 are higher than the catalog values by 3.3 to 4.7%. The obtained percentage elongations for additional material 18/8/6 are higher by 4 to 7%. These deviations are a consequence of mixing the additional material with the basic material (Miletić et al, 2020; Zhang et al, 2015; Durmusoglu et al, 2015).

Comparing the values from Table 9 with the values of the yield stress and the tensile strength of the base materials (Table 7) and the weld metal (Table 8) for plate 1, it can be established that the point A in Figure 7 corresponds to the yield strength of high alloy steel, the point B corresponds to the yield stress of microalloyed steel and the point C corresponds to the tensile strength of high-alloy steel. This is expected according to (Sankar et al, 2021), since high-alloy steel has the lowest yield stress and plastic deformation will start in it first (point A). As the tensile force increases, the yield stress of the microalloyed steel (point B) is reached. The fracture occurred in high-alloy steel at a stress corresponding to its tensile strength (point C). The weld metal has a yield stress significantly higher than the yield stress of high-alloy, but a lower yield stress than microalloyed steel (Zhang et al, 2015; Durmusoglu et al, 2015). Therefore, the weld metal will deform before the point B is reached. As the weld metal and high-alloy steel are of similar structure, they will behave similarly when deformed, so there will be no discontinuity in the σ – ε diagram. The results shown in Table 10 show a good agreement between the voltages in the second and fourth columns, which confirms the assumptions made.

Comparing the values from Table 11 with the values of the yield stress and the tensile strength of the base materials (Table 7) and the weld metal (Table 8) for plate 2, it can be established that the point A in Figure 10 corresponds to the yield strength of high alloy steel and the point B corresponds to the yield stress of microalloyed steel, but it is slightly pronounced in the figure, which distinguishes this diagram from the diagram obtained for plate 1 (Figure 7). The point C corresponds to the tensile strength of microalloyed steel. This sequence is possible, since high-alloy steel has the lowest yield stress and plastic deformation will first begin in it (Miletić et al, 2020; Zhang et al, 2015; Durmusoglu et al, 2015; Sankar et al, 2021) (point A). With the increase of tensile force, the high-alloy steel is strengthened and the yield stress of the micro-alloy steel is reached (point B). Fracture occurs in the microalloyed steel at a stress corresponding to its tensile strength (point C). The weld metal has a yield stress significantly higher than the yield stress of the high-alloy steel, but a slightly lower one than that of the microalloyed steel. According to the values from Tables 7 and 8, the tensile strength of the metal welds is higher than the tensile strengths of the basic materials. Therefore, the weld metal will deform before the point B is reached, as seen in Figure 11. As the weld metal and the high-alloy steel are of similar structure, they will behave similarly when deformed. Table 12 shows a good voltage matching in the second and fourth columns, which confirms the assumptions made.

Conclusions

When welding, it is recommended to use a lower amount of heat input, as this results in a lower degree of mixing the additional material with the base materials. Comparing the obtained results using austenitic additional material MIG 18/8/6 and lower heat input, we obtained a welded joint with superior mechanical characteristics, which ensures better work in all atmospheric conditions.

When cracks are found in the metal weld between the roof covering and the reservoir sheath, this joint is not the weakest point in the welded joint, because plastic deformations of the metal weld start only at stresses at which the basic materials break. The contraction of the weld metal increases with increasing the distance from its axis. The contraction at the same distance to the left and right of the axis of the weld metal is not the same and depends on the characteristics of the steel with which the weld metal is in contact.

The hardness measurements showed that, in all cases, the highest values were found in the HAZ towards the microalloyed base material, and the lowest values were in the HAZ towards the high alloyed base material.

References

Bukvić, A. 2012. *Research of the influence of additional materials on the behavior of ferritic austenitic welded joints*. Ph.D. thesis. Belgrade: University of Belgrade - Faculty of Mechanical Engineering (in Serbian).

Durmusoglu, Ş., Türker, M. & Tosun, M. 2015. Effect of welding parameters on the mechanical properties of GMA-welded HY-80 steels. *Materials Testing*, 57(10), pp.866-871. Available at: https://doi.org/10.3139/120.110797.

Guo, Y., Collins, D.M., Tarleton, E., Hofmann, F., Tischler, J., Liu, W., Xu, R., Wilkinson, A.J & Britton, T.B. 2015. Measurements of stress fields near a grain boundary: Exploring blocked arrays of dislocations in 3D. *Acta Materialia*, 96, pp.229-236. Available at: https://doi.org/10.1016/j.actamat.2015.05.041.

-Jesenice Ironworks. 2005. *Additional welding materials, catalog*. Jesenice Ironworks.

Jovičić, R., Ažman, S., Popović, O. & Prokić–Cvetković, R. 2006. Prednosti primene čelika NIOMOL 490 K pri izradi skladišnih rezervoara za naftne derivate. *Energija*, 7(3-4), pp.66-69 (in Serbian).

Kassner, M.E. 2015. *Fundamentals of Creep in Metals and Alloys, 3rd Edition*. Elsevier & Butterworth-Heinemann. ISBN: 9780080994277.

Liu, D. & Pons, D.J. 2017. Physical-mechanism exploration of the low-cycle unified creep-fatigue formulation. *Metals*, 7(9), art.ID:379. Available at: https://doi.org/10.3390/met7090379.

Liu, D. & Pons, D.J. 2018. Crack Propagation Mechanisms for Creep Fatigue: A Consolidated Explatation of Fundamental Beaviours from Inititation to Failure. *Metals*, 8(8), art.ID:623. Available at: https://doi.org/10.3390/met8080623.

Miletić, I., Ilić, A., Nikolić, R.R., Ulewicz, R. Ivanović, L . & Sczygiol, N. 2020. Analysis of Selected Properties of Welded Joints of the HSLA Steels. *Materials*, 13(6), art.ID:1301. Available at: https://doi.org/10.3390/ma13061301.

Sankar, N., Malarvizhi, S. & Balasubramanian, V. 2021. Mechanical properties and microstructural characteristics of rotating arc-gas metal arc welded carbon steel joints. *Journal of the Mechanical Behavior of Materials*, 30(1), pp.49-58. Available at: https://doi.org/10.1515/jmbm-2021-0006.

Zhang, X-Z., Zhao, M-S., Chiew, S-P., Lee, C-K. & Fung, T-C. 2015. Influence of welding on the strength of high performance steels. In: *7th Asia Pacific Young Researchers and Graduates Symposium (YRGS 2015),* Kuala Lumpur, Malaysia, August 20-21 [online]. Available at: https://hdl.handle.net/10356/80558 [Accessed: 1 Feabruary 2022].

ТЕРМИЧЕСКОЕ ВОЗДЕЙСТВИЕ НА ФИЗИКО-МЕХАНИЧЕСКИЕ СВОЙСТВА АУСТЕНИТНО-ФЕРРИТНЫХ СВАРНЫХ ШВОВ

Александар Г. Буквич[а], **корресподент**, *Далибор* П. Петрович[а],
Игор З. Радисавлевич[б], *Саша* С. Димитрич[а]

[а] Университет обороны в г. Белград, Военная академия,
 г. Белград, Республика Сербия

[б] Министерство обороны Республики Сербия, Военно-технический
 институт, г. Белград, Республика Сербия

Резюме:

Введение/цель: Во время эксплуатационных испытаний резервуаров для хранения бензина в сварном аустенитно-ферритном соединении могут образоваться трещины, что может испортить весь резервуар.

Методы: С целью достижения удовлетворительной прочности и долговечности сварного соединения в данной статье анализируется воздействие подведенного тепла на растяжение сварных соединений. В существующей литературе и на практике дополнительные материалы для сварки элементов резервуара подбираются в соответствии с химическим составом элементов основных материалов с помощью диаграммы Шеффлера. В данной статье описаны характеристики сварных соединений резервуаров для хранения бензина, большая часть которых изготовлена из мелкозернистой микролегированной стали NIOMOL 490 K, а часть крышки резервуара изготовлена из аустенитной стали. Сварка плит, изготовленнных из этих двух материалов, производится методом MIG с дополнительным материалом MIG 18/8/6 при разном количестве подведенного тепла.

Выводы: На основании результатов, полученных при испытании на растяжение в соответствии со стандартом SRPS EN ISO 6892-1:2020, сделан вывод, что поведение соединения в целом зависит от свойств каждой отдельной части сварного соединения и их взаимодействия. Также был сделан вывод, что взаимодействие будет лучше, если сварка выполняется с меньшим количеством подведенного тепла, поскольку в таком случае дополнительные материалы в меньшей степени смешиваются с основными материалами.

Ключевые слова: ферритно-аустенитный сварной шов, твердость, пластичность.

УТИЦАЈ УНЕТЕ ТОПЛОТЕ НА ЗАТЕЗНЕ КАРАКТЕРИСТИКЕ АУСТЕНИТНО-ФЕРИТНИХ ЗАВАРЕНИХ СПОЈЕВА

Александар Г. Буквић[а], **аутор за преписку**, *Далибор* П. Петровић[а],
Игор З. Радисављевић[б], *Саша* С. Димитрић[а]

[а] Универзитет одбране у Београду, Војна академија,
   Београд, Република Србија
[б] Министарство одбране Републике Србије, Војнотехнички институт,
   Београд, Република Србија

ОБЛАСТ: машинство, машински материјали
ВРСТА ЧЛАНКА: оригинални научни рад

Сажетак:

Увод/циљ: Током експлоатацијских испитивања резервоара за складиштење бензина, у аустенитно-феритном завареном споју могу настати прслине што може компромитовати цео резервоар.

Методе: Ради постизања завареног споја задовољавајуће чврстоће и трајности, у раду је анализиран утицај уноса топлоте на затезне карактеристике заварених спојева. У досадашњој пракси додатни материјали за заваривање елемената резервоара бирају се према хемијском саставу елемената основних материјала, а уз помоћ Шефлеровог дијаграма. У овом раду испитиване су карактеристике заварених спојева резервоара за складиштење бензина. Највећи део резервоара израђен је од ситнозрног микролегираног челика NIOMOL 490 K, док је кровни део резервоара израђен од аустенитног челика. Плоче од ова два материјала заварене су MIG поступком са додатним материјалом MIG 18/8/6, при различитим количинама унете топлоте.

Закључак: Анализом резултата добијених испитивањем на затезање, према стандарду SRPS EN ISO 6892-1:2020, закључено је да понашање споја као целине зависи од особина сваког појединачног дела завареног споја и од њиховог међусобног утицаја. Такође, закључено је да је међусобни утицај ефикаснији уколико се заваривање врши нижом количином топлоте, јер се тада остварује мањи степен мешања додатног материјала са основним материјалима.

Кључне речи: аустенитно-феритни заварени спој, чврстоћа, пластичност.